ON ESTIMATING DE-SPECKLED AND SPECKLE COMPONENTS FROM B-MODE ULTRASOUND IMAGES

José C. Seabra and João M. Sanches

Instituto de Sistemas e Robótica / Instituto Superior Técnico
Av. Rovisco Pais, Torre Norte
1049-001 Lisboa, Portugal

ABSTRACT

The information encoded in ultrasound speckle is often discarded but it is widely recognized that this phenomenon is dependent of the intrinsic acoustic properties of tissues. In this paper we propose a robust method to estimate the de-speckled and speckle components from the ultrasound data with the purpose of tissue characterization. A de-speckling method, which can conveniently work with either Radio Frequency (RF) or B-mode data, contributes to an improvement on the visualization of anatomical details, while providing useful fields from where echogenicity and texture features can be extracted. The adequacy of the RF image retrieval and de-speckling methods are tackled using both synthetic and real ultrasonic data.

Index Terms— Ultrasound Speckle, Rayleigh, RF Image Retrieval, De-speckling, Tissue Characterization

1. INTRODUCTION

Ultrasound speckle [1] arises from the coherent accumulation of random scatterers within a resolution cell when a certain anatomical region is scanned. The common model for speckle formation assumes a large number of scatterers whose signals sum with a geometry resembling a random walk of component phasors. This condition, known as *fully developed speckle*, determines Rayleigh statistics for the envelope of the backscattered signal [2]. Regarding image appearance, the Rayleigh distribution is appropriated in homogeneous tissue areas, while other distributions such as K- [3], Nakagami [4], and Rician Inverse Gaussian [2] are more convenient when the imaging region presents strong isolated scatterers, which happens near edges/transitions. Many research work has been developed aiming at providing clearer images for visualization [5]. However, very few publications take into account the pre-processing operations of most scanners which significantly affect the signal properties [3]. Moreover, several authors explore exclusively the extraction of echo-morphology and texture features for tissue diagnosis [6]. This paper proposes a joint method comprising RF image retrieval, de-speckling and speckle isolation (see Fig.1). This method provides useful de-speckled and speckle components (images) from which echogenicity[1] and texture features for tissue characterization can be extracted.

This work was supported by Fundação para a Ciência e a Tecnologia (ISR/IST plurianual funding) through the POS Conhecimento Program which includes FEDER funds.

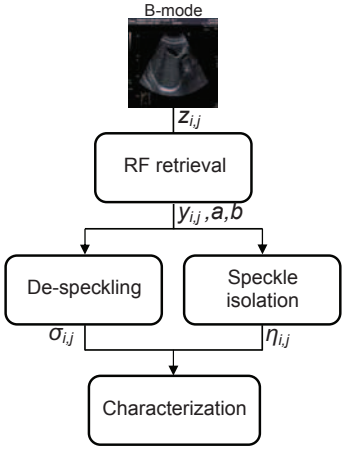

Fig. 1. Architecture of the proposed speckle decomposition method.

2. METHODS

In this section we describe the methods to estimate the envelope RF image from its B-mode version and subsequently we estimate the de-speckle and speckle components.

2.1. RF image retrieval

De-speckling is employed in RF images, which correspond to the envelope of the RF data after polar to cartesian coordinate transformation. The process of RF image retrieval starts with images displayed by the scanner (B-mode images, see Fig. 1). This preliminary procedure is of extreme importance because

[1] Echogenicity is the characteristic ability of a tissue to reflect sound waves and produce echoes.

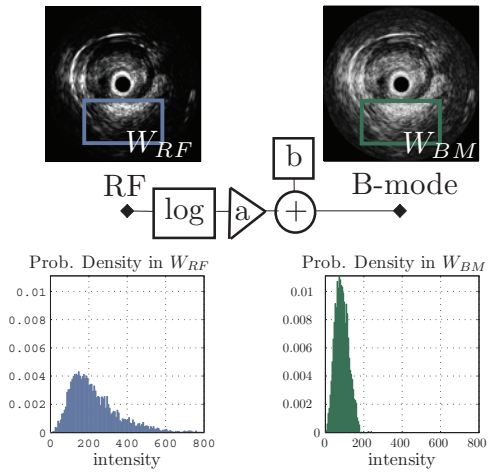

Fig. 2. Block diagram of a generic ultrasound imaging system.

of the significant variability in the appearance of images obtained with different scanners or acquired under different conditions.

A realistic model of the ultrasound image formation process is here proposed (Fig. 2) featuring the most significant operations which affect the signal properties, specifically the logarithmic compression, contrast and brightness tuning. The model, represented in Fig. 2 and designated as *Log-Compression law*, allows to simulate the generic processing operations of the equipment and it is used in the envelope RF image estimation.

Given the assumption of *fully developed speckle*, the envelope RF image, $Y = \{y_{i,j}\}$, is modelled by Rayleigh statistics, where the probability density function (PDF) is given by:

$$p(y_{i,j}) = \frac{y_{i,j}}{\sigma^2_{i,j}} e^{-\frac{y^2_{i,j}}{2\sigma^2_{i,j}}}. \tag{1}$$

The underlying parameter of the Rayleigh distribution, $\mathbf{\Sigma} = \{\sigma_{i,j}\}$, associated with each pixel intensity of the RF image, $y_{i,j}$, is related to the acoustic properties at the corresponding location (i,j), in particular, the so-called echogenicity. Let $\mathbf{Z} = \{z_{i,j}\}$ be a $N \times M$ B-mode image corrupted by speckle where each pixel is generated according to the following *Log-Compression law*:

$$z_{i,j} = a \log(y_{i,j} + 1) + b, \tag{2}$$

where (a, b) are unknown parameters which account for the contrast and brightness respectively. Given (1), the distribution of the observed pixels z, $p(z) = \left|\frac{dy}{dz}\right| p(y)$ is:

$$p(z_{i,j}) = \frac{y_{i,j}(y_{i,j}+1)}{a\sigma^2_{i,j}} e^{-\frac{y^2_{i,j}}{2\sigma^2_{i,j}}}, \tag{3}$$

where $y = e^{\frac{z-b}{a}} - 1$. As pointed out in [7], (3) defines a double exponential distribution with known *standard deviation* (SD) analytical expression [8], yielding an estimate for a:

$$\hat{a}_{i,j} = \sqrt{24}\frac{\sigma_z(i,j)}{\pi}, \tag{4}$$

where $\sigma_z(i,j)$ is the SD of the observations inside the window w, centered at the $(i,j)^{th}$ pixel.

To estimate the parameter b, we first consider the minimum of the observed pixels $z_{i,j}$ given by:

$$\begin{aligned} s = \min\{z_{i,j}\} &= a \log(\min\{y_{i,j}\}+1) + b \\ &= a \log(t+1) + b, \end{aligned} \tag{5}$$

which means that:

$$b = s(\mathbf{Z}) - a \log(t(\sigma, L) + 1), \tag{6}$$

with $\mathbf{Z} = \{z_{i,j}\}$. The distribution of b, derived in [9], is:

$$p(b|s(\mathbf{Z}), \sigma) = \frac{L}{a\sigma^2} t(t+1) e^{-\frac{L}{2\sigma^2}t^2}, \tag{7}$$

where $t = e^{\frac{s-b}{a}} - 1$. An estimator of b is found by computing the expected value of $b_{i,j}$ using a numerical approach, such that:

$$\hat{b}_{i,j} = \sum_{k=1}^{L} b_{i,j}(k) p(b_{i,j}(k)|s, \sigma 0_{i,j}), \tag{8}$$

where $b_{i,j}(k) = k\, s/(L-1)$ and $k = 0, 1, ..., L-1$ are L uniformly distributed values in the interval $[0, s]$, since $b \geq 0$ and from (6), $b \leq s$. In (8), $\sigma 0_{i,j} = \sqrt{\frac{1}{2nm}\sum_{k,l} y0^2_{k,l}}$ is the *Maximum Likelihood* (ML) estimation of $\sigma_{i,j}$ from the pixels inside the window w, $y0_{k,l}$.

The estimators of a and b, considered constant across the image, are obtained by averaging the estimates $\hat{a}_{i,j}$ and $\hat{b}_{i,j}$, such that: $\hat{a} = \frac{1}{NM}\sum_{i,j=1}^{N,M} \hat{a}_{i,j}$ and $\hat{b} = \frac{1}{NM}\sum_{i,j=1}^{N,M} \hat{b}_{i,j}$. These parameters $(\hat{a}, \hat{b})$ are used to retrieve the envelope RF image according to:

$$y_{i,j} = e^{\frac{z_{i,j} - \hat{b}}{\hat{a}}} - 1. \tag{9}$$

2.2. De-speckling

In this section we describe the procedure to estimate the de-speckled image $\mathbf{\Sigma} = \{\sigma_{i,j}\}$ from the estimated envelope RF image, $\mathbf{Y} = \{y_{i,j}\}$. A Bayesian framework with the *Maximum a Posteriori* criterion (MAP) is adopted to deal with the ill poseness nature of the problem. Hence, the de-speckled image is obtained by minimizing an energy function:

$$\hat{\mathbf{\Sigma}} = \arg\min_{\mathbf{\Sigma}} E(\mathbf{Y}, \mathbf{\Sigma}), \tag{10}$$

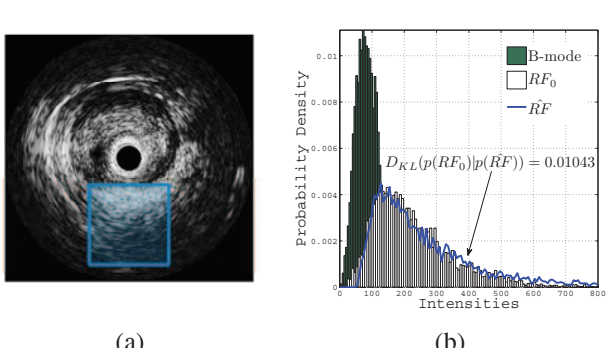

Fig. 3. Speckle decomposition validation using a B-mode IVUS image (a) and corresponding RF_0 image (obtained from original RF signal). PDFs computed in a marked region extracted from B-mode, RF_0 and $\hat{RF}$ images. (c) SNR $(\mu(\eta)/\sigma(\eta))$ map computed over the speckle field $\hat{\eta}$.

where $E(\mathbf{Y}, \mathbf{\Sigma}) = E_d(\mathbf{Y}, \mathbf{\Sigma}) + E_p(\mathbf{\Sigma})$. $E_d(\mathbf{Y}, \mathbf{\Sigma})$, called *data fidelity* term, pushes the solution toward the data and $E_p(\mathbf{\Sigma})$, called *prior* term, regularizes the solution by introducing prior knowledge about $\mathbf{\Sigma}$. The *data fidelity* term is the *log-likelihood* function, $E_d(\mathbf{Y}, \mathbf{\Sigma}) = -\log(p(\mathbf{Y}|\mathbf{\Sigma}))$ where $p(\mathbf{Y}|\mathbf{\Sigma}) = \prod_{i,j=1}^{N,M} p(y_{i,j}|\sigma_{i,j})$ and $p(y_{i,j}|\sigma_{i,j})$ is given in (1). The overall energy function obtained after considering the variable change $x = \log(\sigma^2)$ is:

$$E(\mathbf{Y}, \mathbf{X}) = \sum_{i,j} \left[\frac{y_{i,j}^2}{2} e^{-x_{i,j}} + x_{i,j} \right] + \alpha TV(\mathbf{X}) \qquad (11)$$

where the prior term,

$$TV(\mathbf{X}) = \sum_{i,j} \sqrt{(x_{i,j} - x_{i-1,j})^2 + (x_{i,j} - x_{i,j-1})^2}, \qquad (12)$$

is the so called *Total Variation* (TV) of $\mathbf{X} = \{x_{i,j}\}$.

This energy function is convex because all of its terms are convex (second derivative is positive) which means that its solution is unique and the global minimum is reachable.

2.3. Speckle isolation

The speckle corrupting the ultrasonic data is multiplicative in the sense that its variance depends on the underlying signal

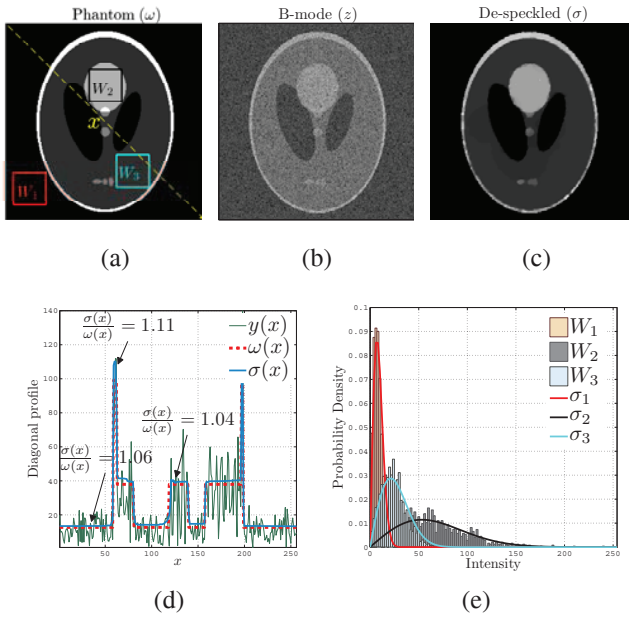

Fig. 4. (a-c) De-speckling example using a phantom image. (d) Diagonal profiles of (a-c). (e) PDFs and data histograms.

$\mathbf{\Sigma}$. Hence, the image formation model may be formulated as follows:

$$y_{i,j} = \eta_{i,j}\sigma_{i,j}, \qquad (13)$$

where $\sigma_{i,j}$ is the intensity of pixel (i, j) of the de-speckled image, while $y_{i,j}$ and $\eta_{i,j}$ are the corresponding pixel intensities in the envelope RF image and speckle field, respectively. The distribution of η is given by:

$$p(\eta_{i,j}) = \left| \frac{dy}{d\eta} \right| p(y) = \eta_{i,j} e^{-\eta_{i,j}^2/2}, \qquad \eta \geq 0, \qquad (14)$$

which is an unit parameter Rayleigh distribution independent of σ. The computation of the speckle field, $\mathbf{N} = \{\eta_{i,j}\}$, is performed from the estimated envelope RF image, $\mathbf{Y} = \{y_{i,j}\}$ and from the de-speckled one, $\mathbf{\Sigma} = \{\sigma_{i,j}\}$ by using (13), yielding:

$$\eta_{i,j} = \frac{y_{i,j}}{\sigma_{i,j}}. \qquad (15)$$

3. EXPERIMENTAL RESULTS

The speckle decomposition method produces a de-speckled image, carrying information about the local tissue echogenicity, and a speckle field, related to the structure and the characteristic pattern of the tissue.

We first investigate the validity of the proposed decomposition method. Hence, we have used an intravascular ultrasound (IVUS) B-mode image corresponding to a cut of the coronary artery (Fig. 3(a)) together with the RF image obtained from raw RF data. The RF image retrieval method

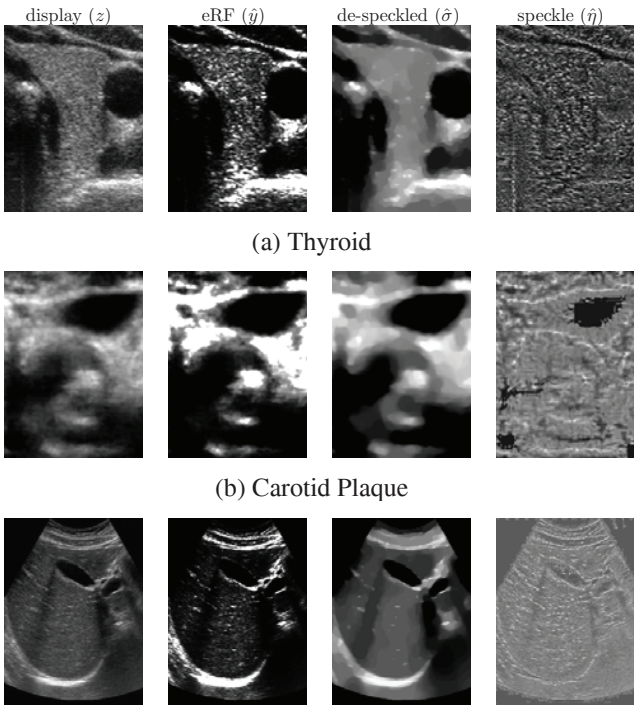

(a) Thyroid

(b) Carotid Plaque

(c) Liver

Fig. 5. Illustrative results of the ultrasound speckle decomposition method applied to different tissue types.

is applied to the B-mode image to obtain an estimated $\hat{RF}$ image. As shown in Fig. 3(b), the statistical properties of the original RF image are closely similar to the ones of the $\hat{RF}$ image. Moreover, using the $\hat{RF}$ image we obtain the de-speckled and speckle components and compute the mean to SD ratio (SNR) across the speckle field η (Fig. 3(c)), whose values, when originated from Rayleigh distribution, should be in the range of 1.5 to 2.5 [1]. Given this, it is observed that the speckle field has statistical properties identical to a Rayleigh distributed signal, which strongly suggests the adequacy of the *Log-Compression law* used for RF image retrieval as well as the Rayleigh observation model for de-speckling.

Secondly, the performance of the de-speckling method is evaluated by use of a phantom image (w) depicted in Fig. 4(a). This image, regarded as containing the true Rayleigh parameters, is corrupted with Rayleigh noise and transformed according to the *Log-Compression law* (2) to obtain a B-mode image Fig. 4(b). After application of the RF image retrieval (providing y) and de-speckling methods, a clean, edge-preserved image is obtained in Fig. 4(c), together with image diagonal profiles of w, y and σ in Fig. 4(d). Moreover, the Rayleigh PDFs obtained with averaged parameters computed in $\sigma(W_1)$, $\sigma(W_2)$, $\sigma(W_3)$ are overlapped with data histograms in $y(W_1)$, $y(W_2)$ and $y(W_3)$.

Fig. 5 exhibits illustrative results of the application of the proposed speckle decomposition method for different tissues, including thyroid (a), carotid plaque (b) and liver (c). Results obtained with synthetic (Fig. 4) and real (Fig. 5) data illustrate the effectiveness and robustness of the de-speckling method to remove speckle while preserving important edges, in images having different properties. Additionally, the adequacy of the algorithm to correctly estimate the Rayleigh local parameters was also established in (Fig. 4(e)).

Although beyond the scope of this paper, we point out two recent studies where ultrasonic tissue characterization was performed using features extracted from de-speckled and speckle components: (i) ultrasonic liver steatosis classification [10] and (ii) subject identification based on ultrasonic thyroid tissue [11].

4. CONCLUSIONS

In this paper, a decomposition procedure is proposed which is able to estimate the de-speckled and speckle components of an ultrasound image, providing additional sources of information, referring to echogenicity and texture. The inclusion of this information in distinct studies here presented showed to be favorable for tissue characterization.

5. REFERENCES

[1] C. Burckhardt, "Speckle in ultrasound B-mode scans," *IEEE Transactions on Sonics and Ultrasonics*, vol. SU-25, no. 1, pp. 1–6, Jan 1978.

[2] T. Eltoft, "Modeling the amplitude statistics of ultrasonic images," *IEEE Transactions on Medical Imaging*, vol. 25, no. 2, pp. 229–240, Feb 2006, Comparative Study.

[3] R. W. Prager, A. H. Gee, G. M. Treece, and L. H. Berman, "Decompression and speckle detection for ultrasound images using the homodyned k-distribution," *Pattern Recogn. Lett.*, vol. 24, no. 4-5, pp. 705–713, 2003.

[4] P.M. Shankar, "Ultrasonic tissue characterization using a generalized Nakagami model," *Ultrasonics, Ferroelectrics and Frequency Control, IEEE Transactions on*, vol. 48, no. 6, pp. 1716–1720, 2001.

[5] Oleg Michailovich and Allen Tannenbaum, "Despeckling of medical ultrasound images," *IEEE Transactions on Ultrasonics, Ferroelectrics, and Frequency Control*, vol. 53, no. 1, pp. 64–78, Jan 2006.

[6] C.I. Christodoulou, C.S. Pattichis, M. Pantziaris, and A. Nicolaides, "Texture-based classification of atherosclerotic carotid plaques," *IEEE Transactions on Medical Imaging*, vol. 22, no. 7, 2003.

[7] J. Seabra and J. Sanches, "Modeling log-compressed ultrasound images for radio frequency signal recovery," in *Proceedings EMBC 2008*, Vancouver, Canada, 2008, IEEE Engineering in Medicine and Biology Society.

[8] Milton Abramowitz and Irene A. Stegun, *Handbook of Mathematical Functions with Formulas, Graphs, and Mathematical Tables*, Dover, New York, ninth dover printing, tenth gpo printing edition, 1964.

[9] J. Sanches and J. Marques, "Compensation of log-compressed images for 3-d ultrasound," *Ultrasound in Medicine and Biology*, vol. 29, no. 2, pp. 247–261, 2003.

[10] Ricardo Ribeiro and João Sanches, "Fatty liver characterization and classification by ultrasound," in *Proceedings of IbPRIA 09*. 2009, pp. 354–361, Springer-Verlag.

[11] J. Seabra and A. Fred, "Towards the development of a thyroid ultrasound biometric scheme based on tissue echo-morphological features.," in *Communications in Computer and Information Science*. 2009, Springer, (to appear).